

SEARCH FOR PERIODIC GRAVITATIONAL WAVE SOURCES WITH THE EXPLORER DETECTOR

P. Astone¹, M. Bassan², P. Bonifazi³, P. Carelli⁴,
E. Coccia², C. Cosmelli⁵, S. D'Antonio⁶, V. Fafone⁶,
S. Frasca⁵, Y. Minenkov², I. Modena²,
G. Modestino⁶, A. Moleti², G. V. Pallottino⁵,
M.A. Papa⁷, G. Pizzella^{2,6}, L. Quintieri⁶, F. Ronga⁶, R. Terenzi³, M. Visco³

¹⁾ *Istituto Nazionale di Fisica Nucleare INFN. Rome, Italy*

²⁾ *University of Rome "Tor Vergata" and INFN. Rome, Italy*

³⁾ *IFSI-CNR. Roma, Italy*

⁴⁾ *University of L'Aquila*

⁵⁾ *University of Rome "La Sapienza" and INFN. Rome, Italy*

⁶⁾ *Laboratori Nazionali di Frascati-INFN. Frascati, Italy*

⁷⁾ *Max Planck Institute for Gravitational Physics, AEI, Germany*

November 12, 2018

Abstract

We have developped a procedure for the search of periodic signals in the data of gravitational wave detectors. We report here the analysis of one year of data from the resonant detector Explorer, searching for pulsars located in the Galactic Center (GC). No signals with amplitude greater than $\bar{h} = 2.9 \cdot 10^{-24}$, in the range 921.32-921.38 Hz, were observed using data collected over a time period of 95.7 days, for a source located at $\alpha = 17.70 \pm 0.01$ hours and $\delta = -29.00 \pm 0.05$ degrees. Our procedure can be extended for any assumed position in the sky and for a more general all-sky search, even with a frequency correction at the source due to the spin-down and Doppler effects.

1 Introduction

Periodic or almost periodic gravitational waves (g.w.) are emitted by various astrophysical sources. They carry important information on their sources (e.g., spinning neutron stars, accreting neutron stars in binary systems) and also on fundamental physics, since their nature can test the model of General Relativity [1, 2]. The main feature of continuous signals which allows them to be detected is that, despite the weakness of the signal (compared to typical amplitudes for bursts), it is possible to implement procedures that build up the signal to noise ratio (SNR) in time. The natural strategy for searching for monochromatic waves is to look for the most significant peaks in the spectrum. In this case the SNR increases with the observation time t_{obs} . In fact, as t_{obs} increases, the frequency resolution of the spectrum also increases - the frequency bin gets smaller $\delta\nu = \frac{1}{t_{obs}}$ - thus the content of the noise power in each bin decreases with t_{obs} , while the signal is not dependent on the length of observation time¹. For a periodic signal of amplitude \bar{h} at the frequency $\bar{\nu}$ the squared modulus of the Fourier Transform provides \bar{h}^2 with a noise contribution of $2 S_h(\bar{\nu}) \delta\nu$, being $S_h(\bar{\nu})$ the two-sided noise power spectrum of the detector (measured in Hz^{-1}).

Thus the SNR for periodic signals is:

$$SNR = \frac{\bar{h}^2 t_{obs}}{2 S_h(\bar{\nu})} \quad (1)$$

Eq.1 holds if the instantaneous frequency of the continuous signal at the detector is known. The analysis procedure in this case is “coherent”, since the phase information contained in the data is used and the sensitivity (in amplitude) increases with the square-root of the time. However in some cases it may be impossible, for various reasons (see later in sect. 3.1), to perform a single Fourier Transform over all the data. This means that the observation time has to be divided in M subperiods, such that the spectral resolution of the spectra becomes $\delta\nu' = M/t_{obs}$ and the corresponding SNR is M times smaller than that given by eq. 1.

The M spectra can be combined together by incoherent summation, that is by averaging the square modulus. In this case the final spectral resolution is again $\delta\nu'$ but there is still some gain as this procedure reduces the variance of the observed noise in the bin. We obtain:

$$SNR' = \frac{\bar{h}^2 t_{obs}}{2 S_h(\bar{\nu}) \sqrt{M}} \quad (2)$$

¹The noise power *density*, i.e. the power spectrum, is independent of t_{obs} , while the signal energy *density* grows with t_{obs}

In general, if the signal is monochromatic but frequency modulated due to the detector-source relative motion, processing techniques exist which can recover the sinusoidal case if the source direction is known. One of the standard ways of detecting such signals is through appropriate resampling of data, better known in the radio astronomy community (where this technique is commonly used) as “data stretching” (see for example [3]). In the case of radio pulsar searches, the location of the source is usually known (the data come from a radio telescope pointing in a particular direction) but some parameters of the system need to be estimated and this is done by a “timing solution which is phase coherent over the whole data set”[3].

However for gravitational waves, especially when searching a large parameter space, it is doubtful that strategies developed for radio pulsar searches can simply be adapted: the expected low SNR values for g.w. signals really modifies the nature of the search strategies that can be employed. In recent ms pulsar searches, for example in [3], the signal is strong enough to allow suspected pulsars to be identified by *visual* inspection of the results of the final stages of the analysis procedure.

For gravitational waves the study of the implementation of optimum analysis procedures is still in progress [4, 5, 6, 7, 8].

In the present analysis, we analyzed the data of the Explorer detector to search for ms pulsars located in the GC, assuming their intrinsic frequency to be constant over the analysis time.

The procedure we used in this study relies on a data base of FFTs, computed from short stretches of data (short with reference to the effects of the Doppler shift, as will be described later in this paper). These short FFTs are then properly combined together to provide a new set of FFTs with higher frequency resolution, representing the signal in the frequency range selected for the study.

The paper is organized as follows: in section 2 we briefly review the characteristics of the detector during the 1991 run, in section 3 we describe the main aspects of the procedure; in section 4 we present the results obtained. The Appendices clarify some aspects of the analysis procedure and discuss the extent to which the constraints that we have introduced to describe the procedure can be relaxed in order to account for different sources.

2 The Explorer detector

The Explorer detector is a cryogenic resonant g.w. antenna located at CERN, at longitude $6^{\circ}12'$ E and latitude $46^{\circ}27'$ N. The apparatus and the experimental set up of the antenna during the 1991 run have been described in [9] and some results of the data analysis for burst detection are given in [10].

The system has two resonance frequencies ($\nu_- = 904.7$ Hz and $\nu_+ = 921.3$ Hz in 1991) where the sensitivity is highest. Fig.1 shows the behaviour

of the two resonance frequencies with time.

Fig.2 shows the hourly averages of the energy sensitivity (SNR=1) to millisecond bursts, expressed as effective temperature T_{eff} in kelvin, obtained with an adaptive Wiener filter ². The relation between T_{eff} and the amplitude of a ms burst is [9] $h = 8 \cdot 10^{-18} \sqrt{T_{eff}}$ (T_{eff} in kelvin).

For periodic waves the sensitivity of a bar detector at the above resonances is given by [12, 13]:

$$\bar{h} = 2.04 \cdot 10^{-25} \sqrt{\frac{T}{0.05 \text{ K}} \frac{2300 \text{ kg}}{M} \frac{10^7}{Q} \frac{900 \text{ Hz}}{\nu_0} \frac{1 \text{ day}}{t_{obs}}} \quad (3)$$

where T is the bar temperature, M its mass, Q the merit factor, ν_0 the resonance frequency of the mode and t_{obs} the observation time. After one year of effective observation, the minimum detectable \bar{h} (amplitude detectable with SNR=1), using the nominal parameters of the Explorer detector ($T = 2 \text{ K}$, $M = 2300 \text{ kg}$, $Q = 10^6$), is

$$\bar{h} = 2 \cdot 10^{-25} \quad (4)$$

in a bandwidth of $\simeq 2 \text{ Hz}$ around the two resonance frequencies and

$$\bar{h} \simeq 2 \cdot 10^{-24}$$

in a bandwidth of 16 Hz between the two resonances. For the NAUTILUS [14] or AURIGA [15] detectors (with $T = 0.1 \text{ K}$, $Q = 10^7$) we get a value $\bar{h} \simeq 1.5 \cdot 10^{-26}$ at the resonances.

3 Main features of the analysis procedure

In the search for continuous signals there are a number of issues that need to be kept in mind regarding the signals that might be present, the apparatus and the quality of the data. As far as the source is concerned, it is not possible to set up a single procedure capable of searching over all types of periodic signals. In this analysis, we concentrated on periodic signals such as those expected from isolated neutron stars with weak spin down, i.e. we ignored the spin down parameters ³. Moreover we did not consider the effects of proper accelerations of the source. Thus our model assumes that the frequency behaviour of the signal exclusively depends on the Doppler effect caused by the motion of our Earth-based detector relative to the source location. Let us quote some basic figures:

²the sensitivity obtained with a matched filter was, on average, better by a factor of two. The comparison between the two filtering procedures is shown in [11].

³however it is possible, using our procedure, to take into account the spin down. This will be the next step in the development of the procedure.

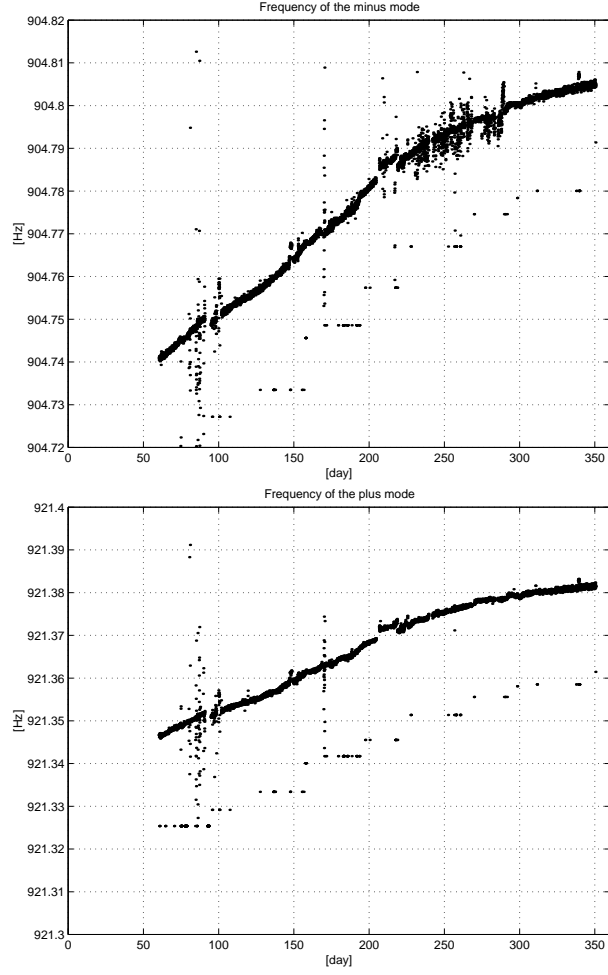


Figure 1: Top: lower resonance (minus mode) frequency against time (in days of the year). Bottom: upper resonance (plus mode) frequency against time. A slow loss in the electrostatic charge of the transducer is probably responsible for the frequency drift

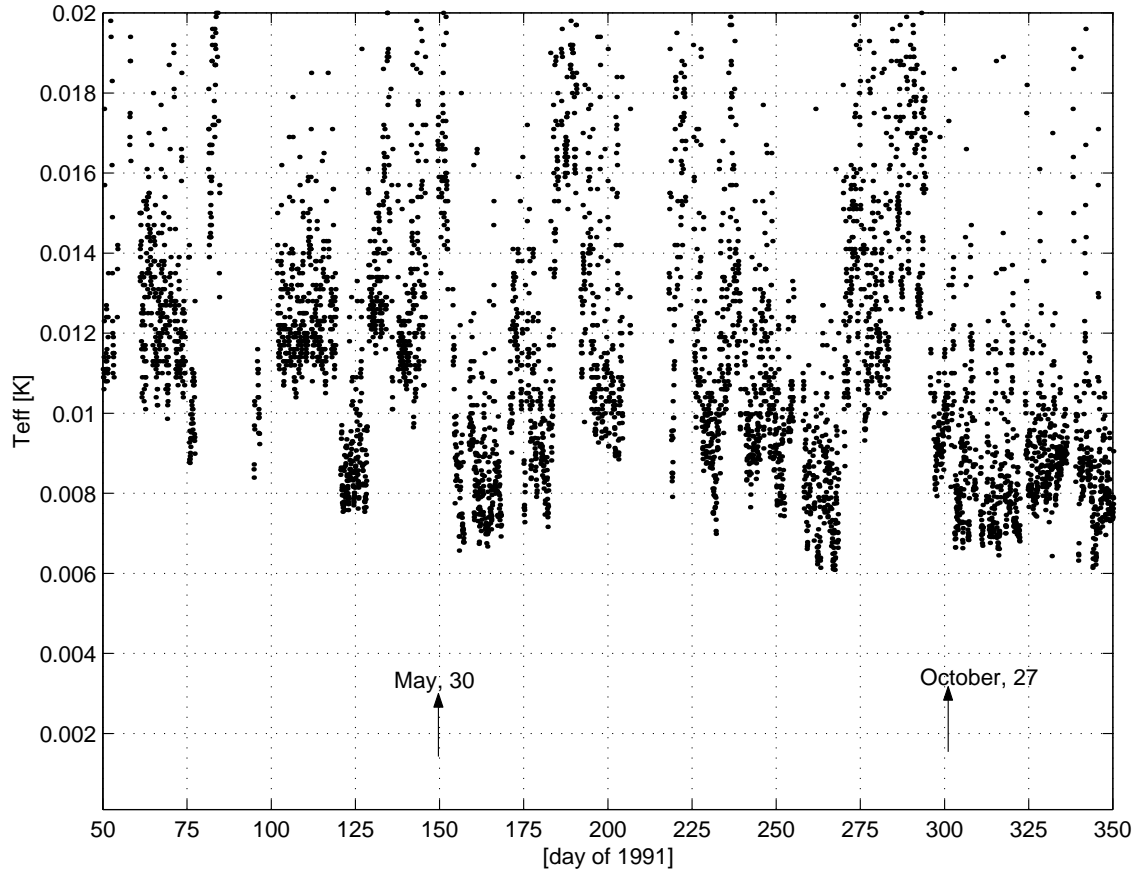


Figure 2: Hourly averages of the Explorer sensitivity to millisecond bursts, expressed as noise temperature (K) as a function of time (in days of the year)

the Doppler effect has two periodic components (see Appendix A). The first one, due to the revolution motion of the Earth over a period of 1 year, produces a maximum spread of

$$\Delta\nu_{rev} = 0.1986 \, \bar{\nu} \cos \beta_{ecl} \text{ mHz} \quad (5)$$

and a maximum time derivative $0.197 \cdot 10^{-10} \, \bar{\nu} \cos \beta_{ecl} \text{ Hz s}^{-1}$ where $\bar{\nu}$ is the intrinsic frequency of the signal and β_{ecl} is the ecliptical latitude of the source. The second one, due to the rotation of the Earth over a period of 1 sidereal day, produces a maximum spread of

$$\Delta\nu_{rot} = 0.00308 \, \bar{\nu} \cos \beta_{ter} \cos \delta \text{ mHz} \quad (6)$$

and a maximum time derivative $1.12 \cdot 10^{-10} \, \bar{\nu} \cos \beta_{ter} \cos \delta \text{ Hz s}^{-1}$. β_{ter} is the terrestrial latitude of the detector and δ the declination of the source.

The observation is also affected by modulation in the amplitude. This is due to the varying orientation of the detector with respect to the source because of the Earth's motion. It may also be a consequence of the polarization of the wave.

As shown, for example, in [16], this modulation spreads the signal power across side bands, spaced at 1/24 hours. The amplitude modulation observed using a resonant bar detector is given by the geometrical part of the detector cross section [17]

$$\Sigma = \Sigma_0 \cdot \Phi(\theta, \epsilon, \phi) = \Sigma_0 \cdot \sin^4 \theta \cdot \left(\frac{1 - \epsilon}{2} + \epsilon \cos^2(2\phi) \right) \quad (7)$$

where ϵ is the percentage of the wave linear polarization ($\epsilon=1$ when there is linear polarization, $\epsilon=0$ when there is no polarization),

$$\Sigma_0 = \frac{16}{\pi} \left(\frac{v}{c} \right)^2 \frac{G}{c} M \quad [m^2 \text{ Hz}]$$

is the (two-sided) mechanical part of the cross section, (M =bar mass, v = sound velocity in the bar), θ is the angle between the bar axis and the wave direction of propagation, ϕ is the angle between the bar axis and the wave polarization plane. The cross section is maximum when the parameters are $\theta = \pi/2, \phi = 0, \epsilon = 1$. If the source location and the polarization state are known, it is possible to demodulate the amplitude of the observed signal.

A major consideration in developing the analysis is that the operation of the detector is not continuous and the noise is not stationary. An example of this is given in Fig.3 which shows power spectra computed over two hours of data in November and September 1991. There are several lines from periodic disturbances which are not stationary, and the noise level differs between the two spectra.

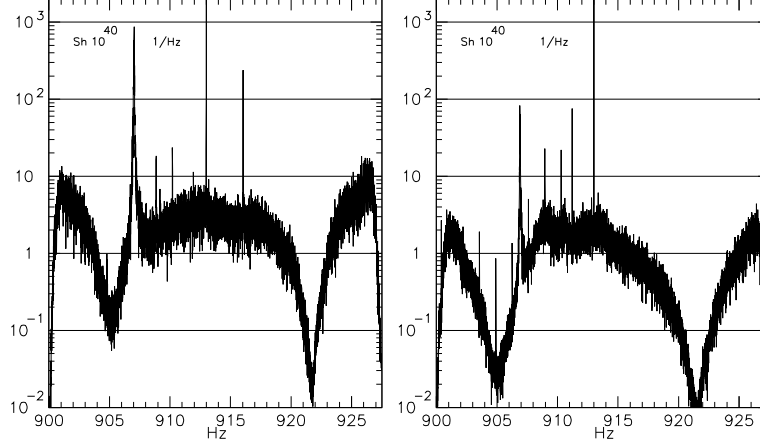


Figure 3: The figure shows two power spectra of the detector, both obtained during periods of “good” operation of the apparatus: during November (left) and September (right) 1991. The y-axis is $S_h \cdot 10^{40}$ in units of $1/\text{Hz}$. The x-axis is the frequency in $[\text{Hz}]$. Comparing the two power spectra, it is easy to see the non stationarity of the system

A final remark needs to be made about the time accuracy required to perform a coherent search over a given time period. A rough calculation, shown in Appendix B, shows that, in a coherent search, the global timing error must be less than $10^{-4} - 10^{-5}$ s/year.

3.1 The length of the FFTs in the data base

Our frequency domain data base consists of “elementary spectra”, each obtained by performing the FFT (Fast Fourier Transform) of a given number of samples of the data, over a duration t_0 , recorded by our detector. The signal sensitivity of each spectrum, according to eq. 1, depends on the duration t_0 . As our observations are affected by the Doppler shift, we have chosen the duration t_0 of the “elementary spectra” to be the longest possible compatible with the requirement that the signal should “appear as monochromatic” during t_0 . This is expressed as:

$$t_{0 \text{ opt}} = \max t_0 \text{ such that } \int_{t_0} \dot{\nu}(t) dt \leq \frac{1}{2t_0}. \quad (8)$$

Clearly some assumptions about the expected $\dot{\nu}$ must be made. In principle, in order to achieve a higher SNR in the short spectrum, some preprocessing could take place by setting a coarse grid on the parameter space (i.e., the part of the sky that is being investigated) and performing suitable data stretching

for each point in that parameter space. In this way a signal coming from that parameter space would appear as monochromatic in the resulting spectrum. As a consequence the dimension of the data base is increased by a factor equal to the number of points in parameter space, but there is a gain in SNR because of the higher spectral resolution.

As stated above, we restricted our analysis to the case where the only frequency changes are due to the Doppler effect of the detector motion relative to the source.

As shown in Appendix A, the time duration must be

$$t_0 < \frac{1}{\sqrt{a+b}} = 8.6972 \cdot 10^4 / \sqrt{\bar{\nu}} \text{ s}, \quad (9)$$

with

$a = \bar{\nu} \cdot 11.244 \cdot 10^{-11} \cos \beta_{ter} \text{ Hz s}^{-1}$ (daily rotation),
 $b = \bar{\nu} \cdot 1.977 \cdot 10^{-11} \cos \beta_{ecl} \text{ Hz s}^{-1}$ (annual orbital motion),
and $\bar{\nu}$ is the source intrinsic frequency.

Thus, to construct the elementary spectra of our data base, we chose a duration of $t_0 = 2382.4 \text{ s} = 39.7 \text{ minutes}$, corresponding to $2N = 131072$ samples, recorded with sampling time of 18.176 ms. With this choice of t_0 , the maximum Doppler frequency variation, $\delta\nu_d = 0.28 \text{ mHz}$, is smaller than the resulting frequency bin $\delta\nu = 0.419 \text{ mHz}$.

3.2 The FFT header

The header of each elementary spectrum of the database contains various information about the original data. This allows stretches of data that are noisier than others to be vetoed or weighted differently and thus best exploits the potential of the data.

Some of the information contained in the header relates to the data structure, some of it to the operational status of the detector and some to data quality. For example, the date and time of the first sample of the data series that the FFT is computed from is stored, along with the frequency resolution of the FFT and the type of time-domain windowing used. There are also system parameters that vary in time: the frequencies of the two modes and of the calibration signal, the level of brownian noise and merit factors at the two modes, the wide band noise level and the status of the operation flags (normal operation, working around the antenna, liquid helium refilling). Some of this information was used to set a threshold for vetoing data (at 40 minutes, which is very reasonable due to typical non stationarities of the detector)

3.3 The procedure for combining spectra

For the targeted search described here the basic FFTs are combined coherently to improve the final sensitivity. The following is an outline of how this is done (details are given in Appendix C).

- take an FFT. Let $\delta\nu$ be the frequency resolution, $2N$ the number of samples and B the bandwidth of the detector;
- take the data from n' bins in the frequency band $\Delta\nu$ of the actual search; $n' = N\Delta\nu/B$;
- build a complex vector that has the following structure:
 - the first datum equal to zero
 - the next n' data equal to those from the selected bins of the FFT
 - zeroes from bins $n' + 1$ up to the nearest subsequent bin numbered with a power of two. Let us say that this way we have n bins.
 - zeroes in the next n bins

So, we end up with a vector that is $2n$ long.

- take the inverse FFT of the vector. This is a complex time series that is the “analytical signal” representation of the signal in the band $\Delta\nu$. It is shifted towards lower frequencies and it is sampled at a sampling rate lower by a factor $2N/2n$ compared to the original time data ⁴. The time of the first sample here is exactly the same as the first datum used for the data base and the total duration is also that of the original time stretch. There are fewer data because the sampling time is longer.
- repeat the steps outlined above for all the M FFTs;
- if they all come from contiguous time stretches simply append one after the other in chronological order. If they are not all contiguous set to zero those stretches where data are missing.
- To correct for the Doppler effect ⁵ from a given source, multiply each sample of the sequence by

$$\exp(-j\phi(t_i)) \tag{10}$$

t_i are the times of the samples and $\phi(t_i) = \int_{t_s}^{t_i} \Delta\omega_D(t)dt$.

$\Delta\omega_D(t)$ is the Doppler correction, in angular frequency, at the time t of the i^{th} sample: $\Delta\omega_D(t) = \omega_D(t) - \omega_s$, where $\omega_D(t)$ is the frequency

⁴ the construction of the analytical signal is a standard procedure of lowpass filtering for a bandpass process. In fact the analytic signal is zero on the left frequency plane, thus avoiding aliasing effects in the lowpass sampling operation [18]

⁵ we could also take into account other causes of frequency shifts such as those affecting the intrinsic frequency of the source.

observed at the detector, due to the Doppler effect from a given source that emits at a constant frequency ω_s . t_s is the start time of the FFT being constructed.

We note that the frequency correction is performed on the subsampled data set, and this is one of the advantages of the procedure.

- Perform the FFT of the $2n \cdot M$ data thus obtained.
- Finally, take the squared modulus of the FFT thus obtained. This is the power spectrum of the original time series, in the band $\Delta\nu$, with the full spectral resolution $\delta\nu/M$. A signal exhibiting frequency variability smaller than the variability we have corrected for, should appear wholly within a single frequency bin, and its resulting SNR will be that of Eq.1

3.3.1 An example of the procedure for combining spectra

The procedure was tested on simulated signals added to the data. We shall now briefly review the results of these tests. Such simulations, although simple in principle, present practical design problems which demand extreme care in the implementation. The simulated signal is constructed in the time domain and then it is handled in exactly the same way as the real detector data (details on the data handling procedures are given in the Appendices). Each FFT of the signal is then added to the corresponding FFT in the data base.

$$s(n\Delta t) = \bar{h}(n\Delta t) \sin(\phi(n\Delta t) + \phi_0) \quad (11)$$

where

Δt is the sampling time, $n = 0, 1, \dots, 131072$, ϕ_0 = initial phase,

$$\phi(n\Delta t) = \int_0^{n\Delta t} \omega_D(t) dt \quad (12)$$

where $\omega_D(t)$ is the frequency at the detector due to the Doppler shift at time t . Using the discrete form of eq.12 we may write the phase at time t_i :

$$\phi_i = \phi_{i-1} + \omega_{Di} \Delta t$$

We report here an example in the absence of noise (we set the detector FFTs to zero, before adding them to the simulated signal).

Fig.4 shows the comparison of the two power spectra obtained from a source assumed to be in the GC, emitting at 921.3 Hz, before and after Doppler removal. It is clear that the spread and the shift in the signal frequency (top figure) have been properly corrected (bottom figure). Here the observation time is 36 hours and the frequency resolution is $6.4 \dots \mu\text{Hz}$.

The level of the signal, after Doppler removal, is that which would be expected ($\bar{h} = 1.0/\sqrt{Hz}$). An accurate analysis of the residual error after Doppler

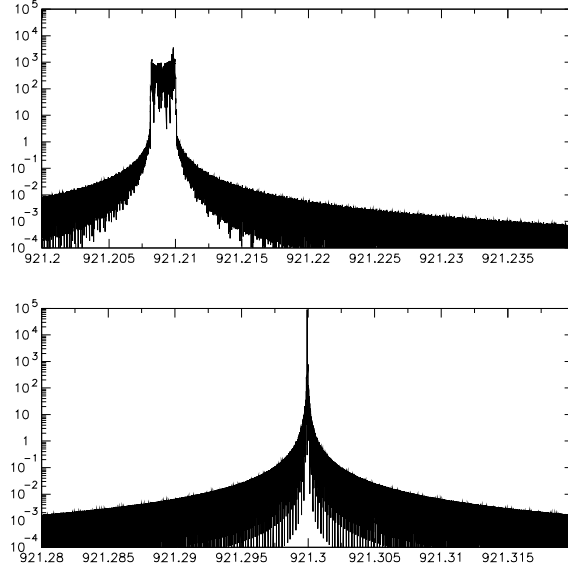


Figure 4: Simulation of a signal (at 921.3 Hz) from the GC, over 36 hours of data. Top: $S_h(\nu)$ of the simulated data. Bottom: $S_h(\nu)$ after Doppler removal. The y-axis is $S_h \cdot 10^{40}$ in units of $1/Hz$. The x-axis is the frequency in [Hz].

removal (this error is defined as the instantaneous difference between the time signal after correction and the time signal in the absence of modulation) showed that this residual error was always less than 0.7%.

4 The analysis of the Explorer data

We analyzed data taken during the period between March and December 1991. These data sets comprise 4954 FFTs from March to July and 4384 from August to December. After a preliminary analysis of the features of the spectra, with particular reference to their sensitivity performance, we decided to veto the spectra with brownian noise larger than 7.8 K (i.e. three times greater than the expected value of 2.6 K [9]), With this criterium we vetoed 807 spectra, that is $\simeq 10\%$ of the total.

A comment on the accuracy of the timing of the data is necessary at this point: the absolute time recording had an indetermination of the order of $10 - 20\text{ ms}$ [9] at the beginning of each new run. This was due to the fact that, although the time was checked against the Swiss time signal HBG with an accuracy of a few ms, the software procedure at the start of each run introduced an imprecision of $\simeq 10 - 20\text{ ms}$.

On the other hand we are confident about the precision of the Rubidium clock, which was used to determine the sampling time. As a consequence we could combine coherently only data obtained from one single acquisition run.

The strategy for the analysis procedure was thus the following:

- choose the frequency bandwidths to be analyzed, and calculate new - higher resolution- FFTs on each new run, for each of these chosen bandwidths
- choose the coordinates of the source location and correct for Doppler effect and for amplitude modulation, using the procedure described in section 3. We ignored possible polarization of the waves.

This analysis was focused on possible sources in the GC, at $\alpha = 17.7$ hours, $\delta = -29.0$ degrees.

To calculate the Doppler shift we used the JPL ephemerides (JPLEPH.405) and software routines from the US Naval Observatory (NOVAS). The amplitude modulation was removed from the data by matched filtering, multiplying the data by the factor $\sin^4 \theta(t)$ (in other words, the data were weighted on the basis of the source-detector direction).

In 1991 we collected data over 51 separate runs and therefore, applying the procedure outlined above, we obtained 51 separate FFTs. Each one has a different frequency resolution, according to its length in time (due to the timing error between different runs). The analysis of the 51 FFTs could only be done by combining their information “incoherently”, thus combining the spectra. Obviously, this reduced the sensitivity of the final analysis (see Eq. 2).

We report here the results of the analysis of the data around the frequency of the plus mode (the mode in Fig.1, bottom).

4.1 The analysis of 95.7 days of data

First of all we give an example using data over one week in June 1991. The observation time is $t_{obs} = 7.05$ days from day 159.8 (June, 8th). The analyzed data are in the bandwidth 921.32-921.38 Hz. The level of the noise is $(1.2 \pm 0.7) \cdot 10^{-24}$, in good agreement with that expected for Explorer (using eq.1, with $T = 2.6$ K and $Q = 10^6$, we get $1.9 \cdot 10^{-24}$)

The Doppler correction needed for signals from the GC was applied to the data. The highest peak is $\bar{h} = 5.2 \cdot 10^{-24}$.

In the case that no Doppler correction was applied to the data there is a very high peak, at the level $\bar{h} = 1.2 \cdot 10^{-23}$, which disappears when the Doppler correction based on a source in the GC is applied. It is most likely that the peak was due to the apparatus. The GC Doppler correction spreads this contribution over several frequency bins.

We started the analysis using only the data from three consecutive runs in May and June.

We averaged the corresponding spectra over a total observation time of $t_{obs} = 21.177$ days from day 128.53 (May, 8th). The analysis was done in the frequency range 921.32-921.38 Hz, where the antenna noise spectral density was flat, as shown in Fig.5. The figure is normalized in terms of the amplitude \bar{h} that would give $SNR = 1$ for sources in the GC. The \bar{h} level is $(1.6 \pm 0.5) \cdot 10^{-24}$. We notice that the average level for the 21.177-day period is roughly (within the observed non stationarities) the same as that for the 7.05-day period, and the standard deviation decreases, as it should do, by a factor of the order of $\sqrt{\frac{21.177}{7.05}} = \sqrt{3}$ (the small difference is due to the non stationarities during the three time periods).

No spectral lines were detected with amplitude (at the detector) greater than $\bar{h} = 4.1 \cdot 10^{-24}$.

To set an upper limit on the amplitude of possible signals from GC in the chosen bandwidth, we decided to check the efficiency of detection, given the noise of the detector. We therefore added signals with different amplitudes and phases to the data, using data without Doppler correction, since the efficiency of detection, on the average, does not depend on the Doppler effect.

We added four different families of signals, each family consisting of 20 sinusoids with the same amplitude but different phases.

Fig.6 shows the histograms. The histograms report the data and the four different families of simulated signals. On the x-axis we have values ranging from $\bar{h} = 1.0 \cdot 10^{-24}$ to $1.6 \cdot 10^{-23}$, with an interval of $0.1 \cdot 10^{-24}$.

The nominal amplitudes of the added signals are $1.4 \cdot 10^{-23}$, $8.7 \cdot 10^{-24}$, $5.8 \cdot 10^{-24}$ and $3.0 \cdot 10^{-24}$. If we consider only the three families of higher signals, the histograms show very clearly that all these signals have been well detected. Even the smallest of these 60 signals is well above the standard

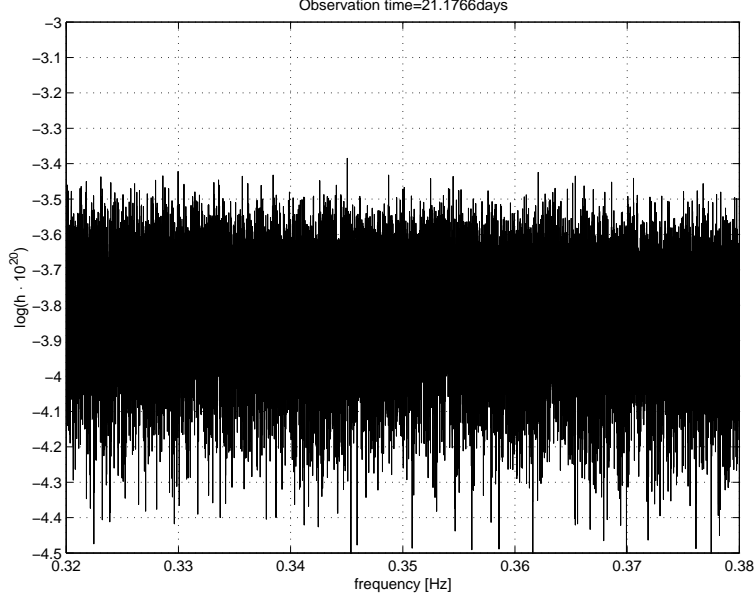


Figure 5: Average \bar{h} from GC obtained averaging the spectra of 3 runs, 7 days each, from May, 8th. The x-axis is the frequency, in Hz-921 Hz.

deviation of the data (the smallest three signals have $\bar{h} = 4.4 \cdot 10^{-24}$, which is roughly 10 times the noise standard deviation). Thus, for these signals, on a time basis of only 21 days, the efficiency of detection is 1. On the contrary, the histograms show that the efficiency of detection for the signals at the lowest level ($3.0 \cdot 10^{-24}$) is very poor.

Thus, on the basis of 21 days of data, we exclude the possibility that, in the GC, there are sources having a spindown age $\tau \geq 3 \cdot 10^7$ years emitting signals with frequency in the range 921.32-921.38 Hz and strength (on Earth) greater than or equal to $\bar{h} = 5.8 \cdot 10^{-24}$.

For the eleven longest runs between May and December the observation times range from 7.7 to 12.8 days, giving a total effective observation time of 95.72 days. We can average these spectra, after adding the necessary zeroes to obtain the same virtual resolution (this produces a change in the SNR and therefore a re-calibration of the spectra is needed).

The start times of these eleven runs, are days 128.53, 137.29, 159.82, 171.43, 213.94, 225.32, 301.61, 312.37, 323.46, 339.68. Fig.7 shows the average \bar{h} for the frequency range 921.32-921.38. In the frequency bandwidth 921.32-921.38 Hz over these 95.7 days the noise level is $(1.2 \pm 0.2) \cdot 10^{-24}$, well in agreement with the expected value. No lines with amplitude greater than $\bar{h} = 2.9 \cdot 10^{-24}$ are apparent.

The standard deviation is a factor 2.5 lower than the standard deviation

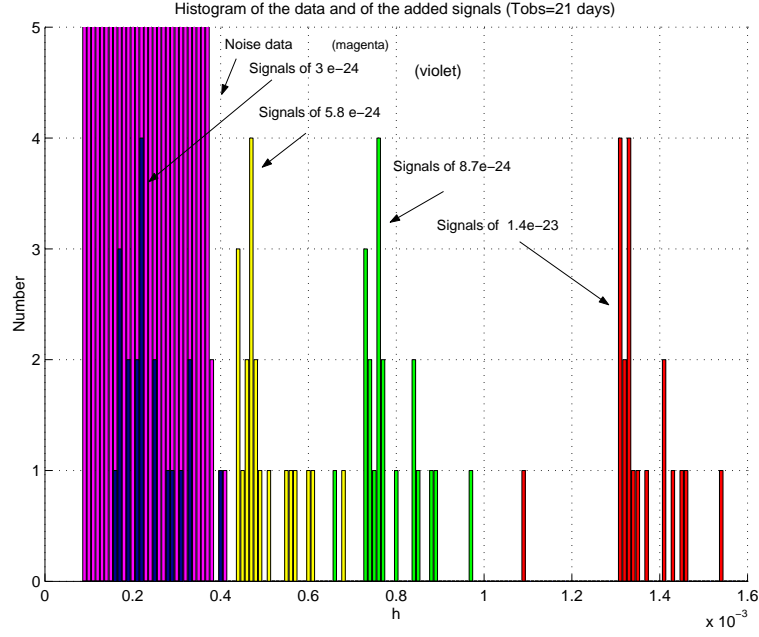


Figure 6: Histograms in the bandwidth 921.32-921.38 Hz. $t_{obs} = 21$ days. The histograms report the data (magenta) and the four different families of simulated signals (violet,yellow,green,red). The y-axis numbers above five have not been plotted. The x-axis ranges from $1.0 \cdot 10^{-24}$ to $1.6 \cdot 10^{-23}$, with interval $0.1 \cdot 10^{-24}$. The histograms show clearly that the efficiency of detection for the simulated signals corresponding to the yellow, green and red plots is 1.

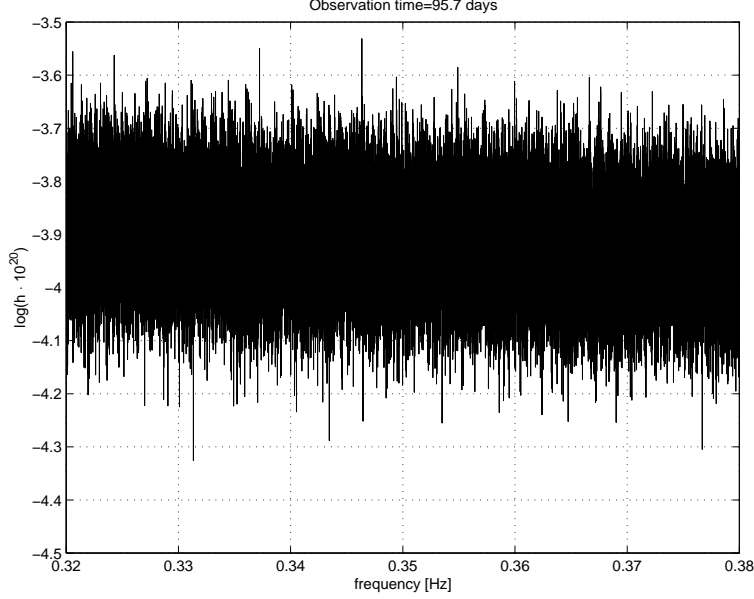


Figure 7: Average \bar{h} from GC obtained using data from May to December (95.7 days) in the bandwidth 921.32-921.38 Hz. The x-axis is the frequency, in Hz-921 Hz

obtained using only 21 days, thus we expect the efficiency of detection over the 95 days be of the order of the unity even for signals of $\bar{h} = 2 - 3 \cdot 10^{-24}$.

Thus, we exclude the possibility that, in the GC, there are sources having a spindown age $\tau \geq 10^8$ years, emitting signals with frequency in the range 921.32-921.38 Hz and strength (on Earth) greater than or equal to $\bar{h} = 2.9 \cdot 10^{-24}$.

4.2 Point registration on the spectra

The analyzed period consists of 51 runs, leading to 51 spectra of different resolution. It is not convenient to average these spectra as done before for the eleven longest ones, because now their duration are very different one from each other. They can be analyzed using various methods- for example, by looking for patterns in the time evolution of their spectral lines. However this kind of analysis would require algorithms which are rather more involved than those used in the present analysis (such algorithms are presently under investigation [4, 5]). The analysis here is also complicated by the fact that the different spectra have different resolutions and thus different SNRs, for any given signal.

We restricted our search to a source in the GC emitting a signal at constant frequency during the observation time. We have tracked all the local maxima in each spectrum obtained by setting a threshold[5] at $\text{SNR} \simeq 4$. If a spectral

line from the GC were present, it should show up in all the spectra (at various SNRs) at the same frequency.

Fig. 8 shows (top) the time-frequency plot of the selected maxima and their histogram (bottom). The resulting histogram is flat and hence no evidence of straight horizontal lines is present in the data. However, as shown in Fig.9, the sensitivity of this analysis is much poorer than the previous method, as almost all these selected maxima have amplitude greater than 10^{-22} .

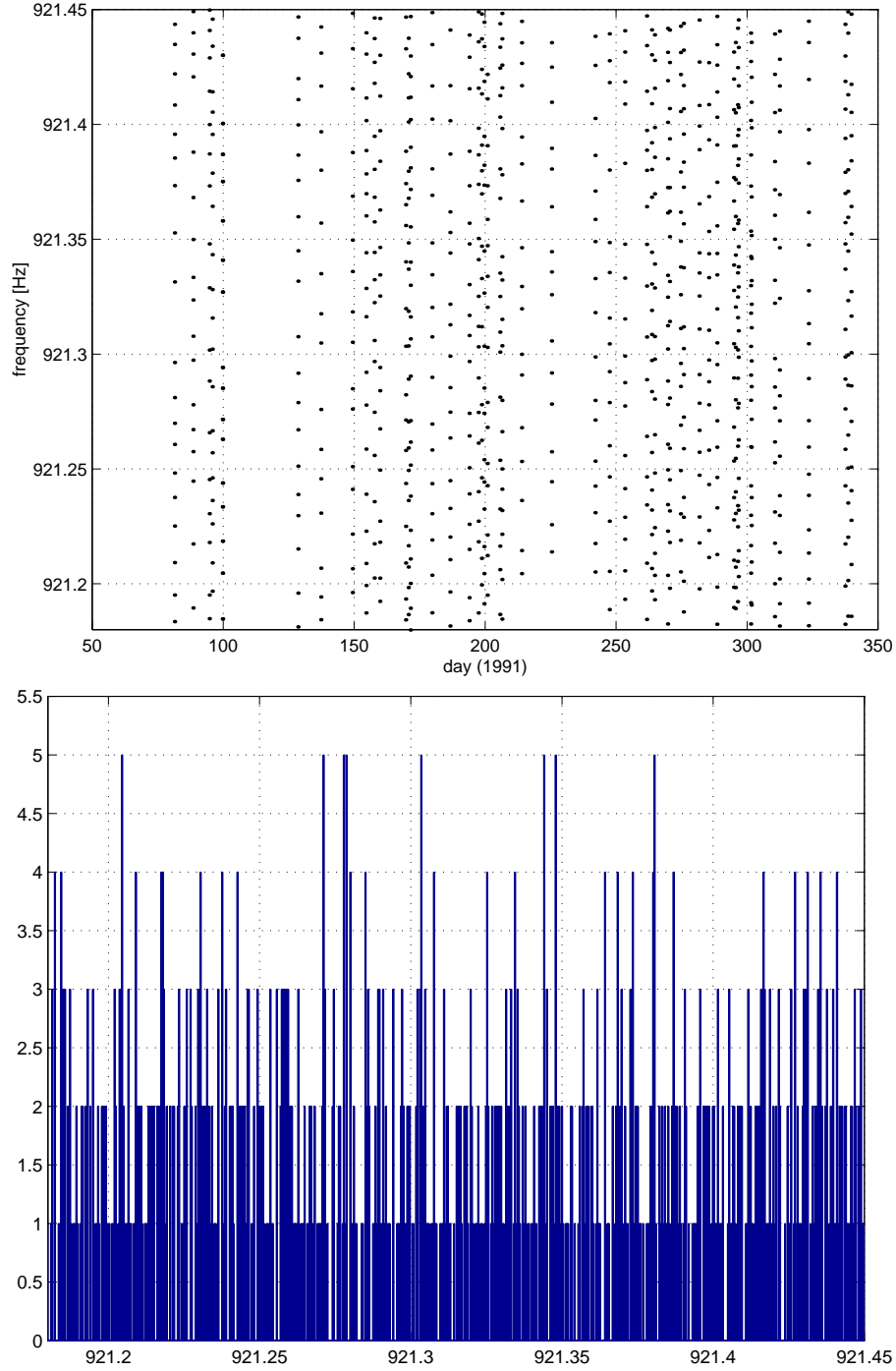


Figure 8: The incoherent analysis over 51 spectra from May to December. The upper plot shows the time-frequency behaviour of the local maxima selected in each spectrum. The lower plot is their histogram versus frequency.

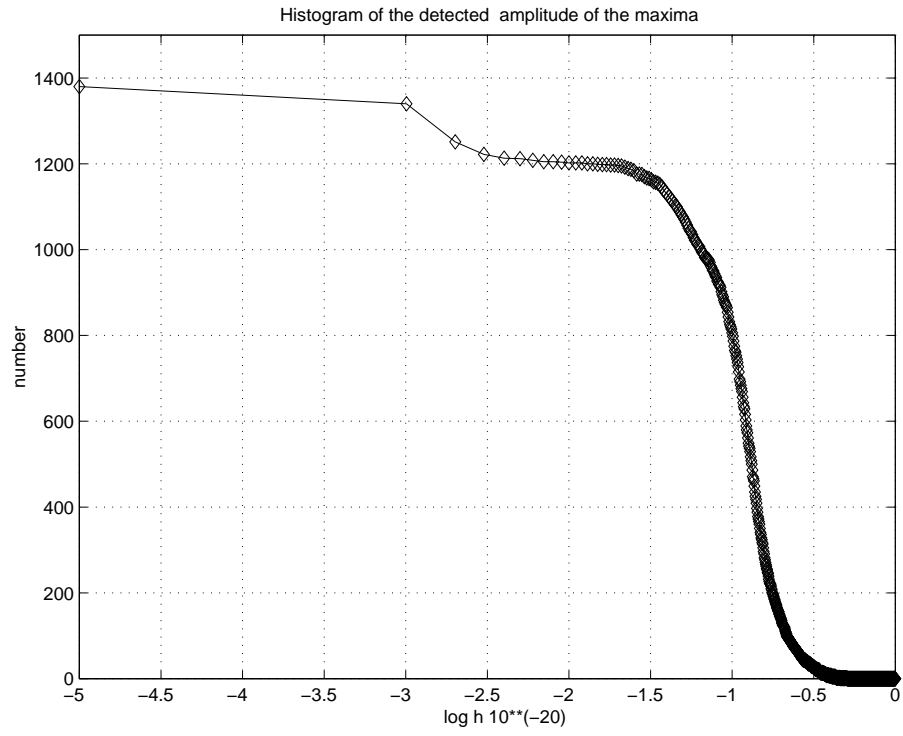


Figure 9: The figure shows the histogram of the (log) amplitudes of the selected local maxima in the 51 spectra

5 Conclusions

A first analysis of the data obtained with the Explorer detector in 1991 was performed, with the aim of searching for continuous g.w.. The analysis was limited to the frequency range 921.32-921.38 Hz, which contained the plus resonance of the detector, where sensitivity was highest. Doppler corrections on the g.w. frequency were made under the assumption that the source was still in the GC without any intrinsic frequency spin down.

No signals were observed with amplitude greater than $\bar{h} = 2.9 \cdot 10^{-24}$, using data collected over 95.7 days, for a source located at $\alpha = 17.70 \pm 0.01$ hours and $\delta = -29.00 \pm 0.05$ degrees, having a spindown parameter $\tau \geq 10^8$ years (that is $\dot{p} \leq 1.7 \cdot 10^{-19}$ s/s).

The procedures adopted here can be applied to any assumed position in the sky of a g.w. source, for a greater frequency range, or even for a frequency correction at the source due to spin down and Doppler effects.

APPENDIX A: Frequency resolution of the basic FFTs

Here we want to show how we chose the spectral resolution for our spectral data base [16, 17].

If $\bar{\nu}$ is the emission frequency of the source then the observed frequency is given by the (simplified) formula

$$\nu = \bar{\nu}(1 \pm (v/c)) \quad (13)$$

where $v = |\vec{v}_{rot} + \vec{v}_{orb}|$ is the relative velocity of the antenna and source, due to \vec{v}_{rot} , daily rotation of the Earth, and to \vec{v}_{orb} , orbital motion around the Sun.

Orbital motion, annual:

$$\vec{v}_{orb} = |v_{orb}| \cdot \cos(\Omega_{orb}t) \quad (14)$$

$$|v_{orb}| = \Omega_{orb}R_0 = 2\pi R_0/T_{orb} = 2\pi R_0/(365 \cdot 86400) = 29.772 \text{ km/s} \quad (15)$$

$$R_0 = 149504201 \text{ km}; \Omega_{orb} = 2\pi/(86400 \cdot 365) = 1.99 \cdot 10^{-7} \text{ rad/s}; |v_{orb}|/c \simeq 0.9933 \cdot 10^{-4}.$$

$$\frac{d\nu_{orb}}{dt} = \bar{\nu} (1/c) \cos \beta_{ecl} \frac{d\vec{v}_{orb}}{dt} \quad (16)$$

$$\frac{d\vec{v}_{orb}}{dt} = R_0 \Omega_{orb}^2 \cdot \cos(\Omega_{orb}t) = \vec{v}_{orb} \Omega_{orb} \quad (17)$$

$$\left. \frac{d\nu_{orb}}{dt} \right|_{max} = \bar{\nu} (|v_{orb}|/c) \cos \beta_{ecl} \Omega_{orb} = \bar{\nu} (|v_{orb}|/c) \cos \beta_{ecl} \frac{2\pi}{T_{orb}} \frac{Hz}{s} \quad (18)$$

$$\simeq \bar{\nu} \cdot 1.9778 \cdot 10^{-11} \cos \beta_{ecl} \frac{Hz}{s} \quad (19)$$

Daily rotation:

$$\vec{v}_{rot} = |v_{rot}| \cdot \cos(\Omega_{rot}t) \quad (20)$$

$$|v_{rot}| = \Omega_{rot}R_T = 2\pi R_T/T_{rot} = 2\pi R_T/86400 = 0.4636 \text{ km/s} \quad (21)$$

$$R_T = 6378.388 \text{ km}; \Omega_{rot} = 2\pi/86400 = 7.2 \cdot 10^{-5} \text{ rad/s}; |v_{rot}|/c \simeq 1.5467 \cdot 10^{-6}.$$

$$\left. \frac{d\nu_{rot}}{dt} \right|_{max} = \bar{\nu} (|v_{rot}|/c) \cos \beta_{ter} \Omega_{rot} = \bar{\nu} (|v_{rot}|/c) \cos \beta_{ter} \frac{2\pi}{T_{rot}} \frac{Hz}{s} \quad (22)$$

$$\simeq \bar{\nu} \cdot 11.244 \cdot 10^{-11} \cos \beta_{ter} \frac{Hz}{s}$$

We will use here the symbols $|\Delta\nu_{max}|_{rot}$ and $|\Delta\nu_{max}|_{orb}$ for the maximum frequency shift, in the time interval ΔT .

$$\frac{|\Delta\nu_{max}|_{rot}}{(\bar{\nu} \Delta T)} = 11.244 \cdot 10^{-11} \cos \beta_{ter} \text{ s}^{-1} \quad (23)$$

if ΔT less than 1 day.

$$\frac{|\Delta\nu_{max}|_{orb}}{(\bar{\nu} \Delta T)} = 1.977 \cdot 10^{-11} \cos \beta_{ecl} \text{ s}^{-1} \quad (24)$$

if ΔT less than 1 year.

$$(|\Delta\nu_{max}/\Delta T|_{rot} + |\Delta\nu_{max}/\Delta T|_{orb}) \cdot T \quad (T < 1 \text{ day}) \quad (25)$$

$$(|\Delta\nu_{max}/\Delta T|_{rot} + |\Delta\nu_{max}/\Delta T|_{orb}) \cdot T < \delta_{\nu_f} \quad (26)$$

$$1/T > T \cdot (a + b)$$

where

$$a = \bar{\nu} \cdot 11.244 \cdot 10^{-11} \cos \beta_{ter} \frac{Hz}{s}, \text{ (daily rotation)}$$

$$b = \bar{\nu} \cdot 1.977 \cdot 10^{-11} \cos \beta_{ecl} \frac{Hz}{s}, \text{ (annual orbital motion)}$$

$$T^2 < 1/(a + b)$$

$$T < 8.6972 \cdot 10^4 / \sqrt{\bar{\nu}} \text{ s}$$

If we consider $\bar{\nu} = 1000 \text{ Hz}$

$$T < 2749.9 \text{ s} \quad (27)$$

In our data, the sampling time is $\delta_{t_f} = 18.176 \text{ ms}$ then, using $T = 2382.35 \text{ s}$, that is 0.6617 hours, we have a frequency resolution

$$\delta_{\nu_f} = 0.41975 \text{ mHz}$$

that is $2^{17} = 131072$ samples in each periodogram.

APPENDIX B: Timing precision

We note here that precision in both the absolute time and the sampling frequency during the observation time t_{obs} is crucial when combining the basic FFTs to construct one very long spectrum.

If ν is the frequency of the wave, $\tau = \frac{1}{\nu}$ the wave period, $\epsilon_\nu = \frac{\Delta\nu}{\nu}$ the relative frequency error ($\Delta\nu$ represents here the wave frequency indetermination due to the acquisition and analysis procedures) then

$$\Delta\tau = \epsilon_\nu \cdot \tau$$

After time t_m we have a phase error of

$$\frac{\Phi}{2\pi} = t_m \Delta\nu = t_m \nu \epsilon_\nu$$

Hence, if we want a phase error $\frac{\Phi}{2\pi} < \simeq 0.01$ in $t_m = 1 \text{ year} = 3.1 \cdot 10^7 \text{ s}$ we need $\epsilon_\nu < \simeq 3 \cdot 10^{-10} \frac{1}{\nu}$

Hence, if $\nu = 1 \text{ kHz}$:

$$\epsilon_\nu < \simeq 3 \cdot 10^{-13}$$

$$\Delta\tau < \simeq 10^{-5} \text{ s/year}$$

APPENDIX C: Practical issues in the construction of the data base

- Each FFT is computed using $2N$ data, sampled with sampling time Δt . The data are windowed, in the time domain, before the Fourier transform. This means that the data y_i are multiplied by $w_i = A - B \cos(i) + C \cos(2i)$, where $i = (0, 2N - 1) \cdot 2\pi / (2N - 1)$. In the present analysis we have used a Hamming window, that is $A = 0.54$, $B = 0.46$ and $C = 0$.
- The FFTs are stored in units of strain/ $\sqrt{\text{Hz}}$, and are normalized so that their squared modulus is the spectrum.
- The basic FFTs of the data base overlap for half their length. The time duration of each FFT is $t_0 = 2N\Delta t$, and a new FFT is done after time $t_0/2$. This is important since it avoids distortions in the final time domain sequence - this is the well known "overlap-add" method, described in many data analysis textbooks. For the Explorer detector we thus have 110 FFTs over 36 hours with $\delta\nu = 0.41... \text{ mHz}$.
- We select the frequency bandwidth to be analyzed and we add zeroes to construct the analytical signal. These data should be to a power of two, to allow use of a Fast Fourier algorithm. The chosen bandwidth should be wide enough to include all the frequencies we expect to observe due to the Doppler shift from the given source, during the time of observation.
- After the bandwidth has been selected, the data (still in the frequency domain) should be windowed, to avoid edge effects in the transformed data.

- The selected data are then transformed to return to the time domain. At this stage we must remove the window used in the data when constructing the FFT data base, by simply dividing the new time domain data by $w(t)$. This operation recovers the original time data (subsampled) because the only regions where the division might not work are the edges of the data stream, where the value of the function $w(t)$ may be zero, depending on the kind of window used (a problem which, of course, has been overcome by the overlapping of the FFTs).
- If an FFT under consideration is vetoed or if it is missing, then the data are set to zero.
- Each new group of time domain data is appended to the previous groups, after elimination of the overlapped data. Since the overlapping concerns half the data we eliminate 1/4 of the data at the beginning and end of each stream. The first 1/4 data in the first FFT and the last 1/4 in the last FFT can be discarded. The data of missing or vetoed periods, set to zero as explained above, are appended to the others in the same way.
- At this stage we have a subsampled time domain data stream, which represents the analytical signal associated with the original data.
- Now we can take into account the Doppler shift and correct the data as previously explained.
- The final step is to calculate the power spectrum from this subsampled time domain data (after data windowing in the time domain)

APPENDIX D: Uncertainty in the source parameters

Uncertainty in the source position parameters

In this analysis we used the coordinates $\alpha = 17.7$ hour, $\delta = -29.0$ deg to define the GC. In order to calculate the region of the sky effectively covered by this definition it was necessary to study the effect on the analysis of a source not being “exactly” in the GC, since the frequency modulation depends on the precise location of the source. To get an idea of the problem in 1991 we plotted (Fig. 10) the difference in the observed frequencies on Earth between a signal from the GC and signals coming from sources at nearby coordinates.

From the graph it is easy to see that a difference in the right ascension of ± 0.01 hours leads to a maximum difference in the observed frequency of $\simeq 2 \cdot 10^{-4}$ Hz. This mismatch is at a maximum twice a year, at the beginning of June and at the beginning of December. Thus, we studied the effect of the mismatch during a run in December, when it was at a maximum.

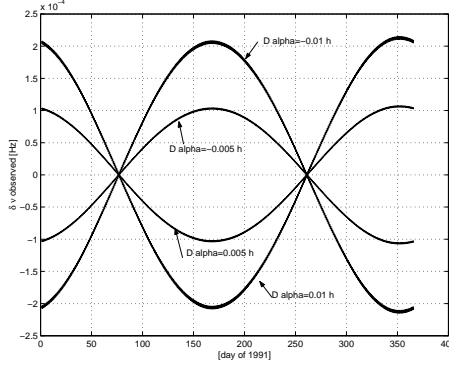


Figure 10: The graph shows the difference in the observed frequency on Earth between a signal in the GC and signals coming from nearby coordinates. The x-axis are days of 1991. The y-axis are the frequencies, from $-2.5 \cdot 10^{-4}$ to $2.5 \cdot 10^{-4}$ Hz

Table I shows the results for uncertainties both in right ascension and in declination. The first column gives the error in right ascension (α in hours); the second, the error in declination (δ in degrees); the third, the energy of the spectrum of the signal, $1/\text{Hz}$, in the frequency bin of its maximum and in the previous and next bins nearest to the maximum; the fourth column gives the difference in the frequency of the signal compared to the nominal, expressed in number of bins (one bin is $8.1 \cdot 10^{-7}$ Hz). Fig.11 is the corresponding 3-dimensional plot. The z-axis is the energy of the signal, integrated over the three bins.

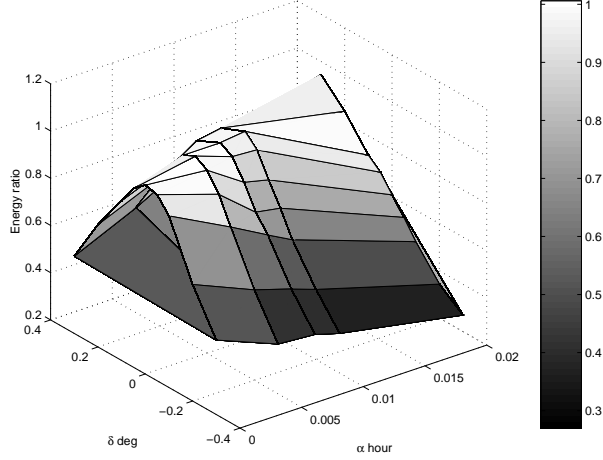


Figure 11: 3-dimensional plot of the data in Table I. The z-axis is the energy of the signal integrated over the three bins (maximum,previous, next). The x and y-axes are the mismatch in right ascension (hours) and in declination (degrees)

It is not easy to arrive at a general conclusion, because the final effect depends on the mismatch on both the parameters and, in some cases, when the two parameters act in opposite direction, the final result is better compared to a mismatch in only one of the two parameters. This is why, for example, the result when $\Delta\alpha=0.01$ hour and $\Delta\delta=0.3$ deg is better than $\Delta\alpha=0.01$ hour and $\Delta\delta=0$ deg. Anyway, assuming the analysis is valid even when there is a worsening by a factor of 2 in SNR we may conclude that the region of the sky under study is definitely within either the volume $\alpha = 17.7 \pm 0.01$ hours and $\delta = -29.0 \pm 0.05$ degrees (0.01 hours=0.15 degrees), or the volume $\alpha = 17.7 \pm 0.005$ hours and $\delta = -29.0 \pm 0.2$ degrees. We also note that the observed frequency shift of the maximum is consistent with that which would be expected (compare, for example, the results in Table I with those in Fig. 10).

Table 1: Results for uncertainties in right ascension and in declination

Table I

$\Delta\alpha$ h ,	$\Delta\delta$ deg ,	signal energy	Δf (n bin)
0.000	-0.30	0.25; 0.31; 0.28	+13
0.000	-0.20	0.24; 0.46; 0.43	+8
0.000	-0.10	0.35; 0.79; 0.37	+4
0.000	-0.05	0.40; 0.95; 0.26	+2
0.000	0.000	0.46; 1.00; 0.17	+0
0.000	+0.05	0.51; 0.92; 0.13	-2
0.000	+0.10	0.56; 0.74; 0.13	-4
0.000	+0.20	0.31; 0.51; 0.35	-9
0.000	+0.30	0.24; 0.33; 0.29	-14
0.005	-0.30	0.26; 0.26; 0.15	+143
0.005	-0.20	0.35; 0.37; 0.23	+139
0.005	-0.10	0.31; 0.59; 0.39	+134
0.005	-0.05	0.40; 0.72; 0.35	+131
0.005	0.000	0.47; 0.85; 0.27	+129
0.005	+0.05	0.50; 0.95; 0.19	+128
0.005	+0.10	0.50; 0.96; 0.14	+126
0.005	+0.20	0.51; 0.66; 0.18	+127
0.005	+0.30	0.29; 0.43; 0.33	+116
0.008	-0.30	0.21; 0.26; 0.18	+220
0.008	-0.20	0.24; 0.34; 0.29	+206
0.008	-0.10	0.43; 0.47; 0.25	+202
0.008	-0.05	0.19; 0.55; 0.52	+199
0.008	0.000	0.18; 0.71; 0.53	+197
0.008	+0.05	0.15; 0.88; 0.52	+195
0.008	+0.10	0.13; 0.96; 0.51	+193
0.008	+0.20	0.23; 0.79; 0.50	+189
0.008	+0.30	0.34; 0.50; 0.35	+184
0.010	-0.30	0.16; 0.23; 0.21	+271
0.010	-0.20	0.26; 0.31; 0.24	+266
0.010	-0.10	0.24; 0.44; 0.38	+261
0.010	-0.05	0.29; 0.56; 0.38	+260
0.010	0.000	0.35; 0.67; 0.36	+255
0.010	+0.05	0.42; 0.79; 0.33	+256
0.010	+0.10	0.43; 0.92; 0.27	+254
0.010	+0.20	0.36; 0.95; 0.24	+250
0.010	+0.30	0.40; 0.59; 0.29	+246
0.020	-0.30	0.11; 0.18; 0.15	+429
0.020	-0.20	0.21; 0.23; 0.12	+426
0.020	-0.10	0.23; 0.30; 0.23	+421
0.020	-0.05	0.29; 0.34; 0.25	+419
0.020	0.000	0.35; 0.40; 0.24	+417
0.020	+0.05	0.43; 0.45; 0.22	+415
0.020	+0.10	0.16; 0.52; 0.49	+412
0.020	+0.20	0.08; 0.68; 0.62	+408
0.020	+0.30	0.64; 0.78; 0.12	+405

Table 2: Results for uncertainty in the source frequency. The first column gives the error in the frequency ($\Delta\nu$ in Hz); ; the second, the energy of the spectrum of the signal, 1/Hz, in the frequency bin of its maximum and in the previous and next bins nearest to the maximum; the third column gives the difference in the frequency of the signal compared to the nominal, expressed in number of bins (one bin is $8.1 \cdot 10^{-7}$ Hz)

Table II

$\Delta\nu$	signal energy	Δf (n bin)
0.0	(0.46) 1.00 (0.17)	+0
+0.1	(0.29) 0.92 (0.39)	+1
-0.1	(0.71) 0.73 (0.15)	-1

Uncertainty in the source frequency

To test the extent to which the analysis depends on knowledge of the intrinsic frequency of the source, we did a simulation of a spectrum of 14.1 days, by introducing a signal at 921.3 Hz and correcting it, during Doppler removal, using 921.2 and 921.4 Hz (that is with an error of ± 0.1 Hz). From Table II it is easy to see that there are no significant differences in the resulting spectra. Thus the final result is only slightly affected by even a very “big” error such as this. This finding is important because it allows us to analyze just a set of discrete frequencies, for example just 1/100 of the frequencies in the original FFTs (0.419... mHz). It can be shown that this property is intrinsic to the

nature of the Doppler correcting factor (eq. 10), which depends on the *difference* between the intrinsic and the observed frequency. Fig.12 shows, for example, the difference (over two years) between the terms $\nu_1 - \nu_{1d}$ and $\nu_2 - \nu_{2d}$, where $\nu_1 = 921.300$ Hz, $\nu_2 = 921.257$ Hz, ν_{1d} and ν_{2d} are the observed frequencies at the detector, assuming the source to be in the GC. This difference is of the order of $3 \cdot 10^{-5}$.

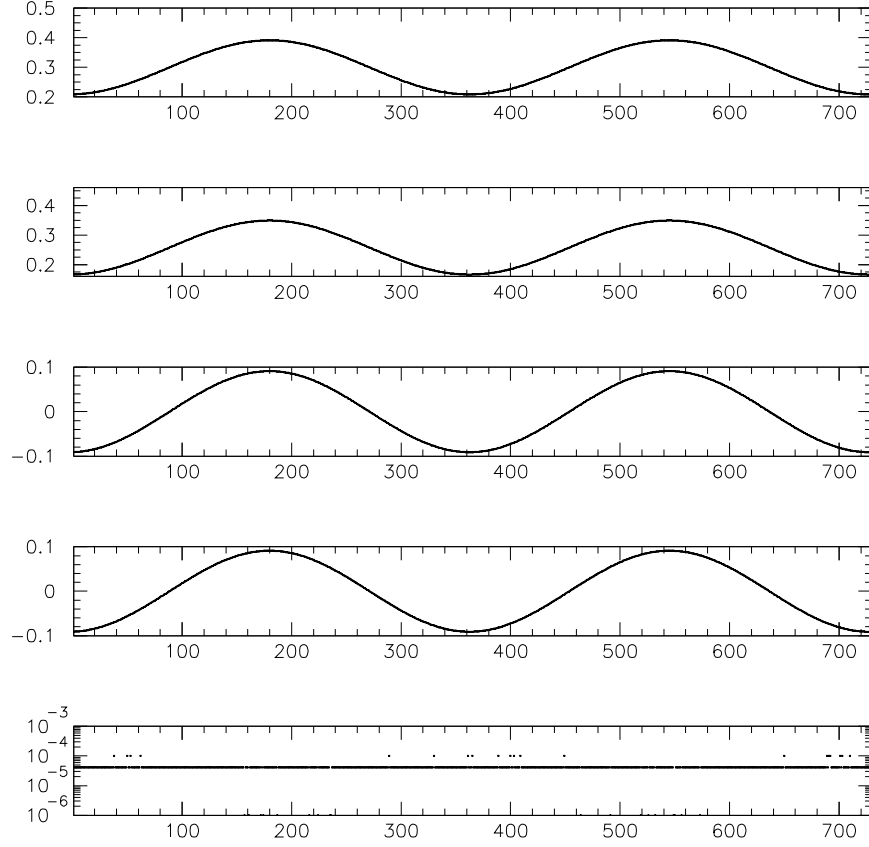


Figure 12: The top figure shows the observed ν_{1d} frequency-921 Hz, assuming a source in the GC emitting at $\nu_1=921.300$ Hz. The x-axis is in days. The second figure shows the same for a signal at $\nu_2=921.257$ Hz. The third and the forth are $\nu_1 - \nu_{1d}$ and $\nu_2 - \nu_{2d}$. The bottom figure is the difference between the third and the fourth figures.

References

- [1] B. F. Schutz
 “Gravitational Waves:The Wager”, Max Plank Institut, AEI-033 April 1997 and Proceed. of the 12th Sigrav meeting, World Scientific (1997).
- [2] K. Thorne
 “Gravitational radiation”, in 300 years of Gravitation (1987)
- [3] F. Camilo, D. R. Lorimer, P. Freire, A. G. Lyne
 “Observation of 20 ms pulsars in 47 Tucanae at 20 cm” The Astrophysical Journal, 535,975-990, 2000, astro-ph/9911234
- [4] C. Cutler, B.F. Schutz,
 “Searching for periodic sources with LIGO”, gr-qc/9702050, Phys. Rev. D 57,2101-2116 (1998).
- [5] M. A. Papa, P. Astone, S. Frasca, B.F. Schutz
 “Searching for continuos waves by line identification” in Albert Einstein Institute AEI-057, February 1998, and Proceed. of the GWDAW2, Orsay (1997).
- [6] A. Krolak,
 “Data analysis for continuous g.w. signals”, gr-qc/9903099
- [7] P. Astone, S. Frasca, M.A. Papa
 “Main features of the proposed short FFT data base and of the analysis procedures that will operate on it”
 “Practical aspects of the proposed targeted search with short FFTs”
 at the “Working group on algorithms for reconstructing data from short FFT data base”, Joint meeting Max Plank Institut of Potsdam and University of Rome ”La Sapienza”, Rome (18 may 1998). (this and related material is available at <http://grwav3.roma1.infn.it/pia/papersweb.html> and <http://grwav1.roma1.infn.it/dadps>)
- [8] P. Brady, T. Creighton, “Searching for periodic sources with LIGO II. Hierarchical searches. gr-qc/9812014. Phys. Rev D61 (2000) 082001
- [9] P. Astone, M. Bassan, P. Bonifazi, P. Carelli, M.G. Castellano, G. Cavallari, E. Coccia, C. Cosmelli, V. Fafone, S. Frasca, E. Majorana, I. Modena, G.V. Pallottino, G. Pizzella, P. Rapagnani, F. Ricci, M. Visco, “Long-term operation of the Rome Explorer cryogenic gravitational wave detector”, Physical Review D **47** 2 (1993) 362-375. From 1998 Explorer is a CERN recognized experiment.
- [10] P. Astone, M. Bassan, P. Bonifazi, P. Carelli, E. Coccia, C. Cosmelli, V. Fafone, S. Frasca, K. Geng, W.O. Hamilton, W. W. Johnson, E. Mauceli,

- M. P. McHugh, S. Merkowitz, I. Modena, P. Modestino, A. Morse, G.V. Pallottino, M. A. Papa, G. Pizzella, N. Solomonson, R. Terenzi, M. Visco, N. Zhu, “Search for gravitational radiation with the Allegro and Explorer detectors” *Physical review D*, vol 59, 122001 (1999)
- [11] P. Astone, C. Buttiglione, S. Frasca, G.V. Pallottino, G. Pizzella, “The fast matched filter for gravitational wave data analysis: characteristics and applications”, *Nota interna Dip. di Fisica “La Sapienza”* n. 1052, 1995 e *Il Nuovo Cimento* **20C** 1 (1997) 9-60.
 - [12] G.V.Pallottino, G.Pizzella “Search for monochromatic g.w. with resonant detectors” *Il Nuovo Cimento* 7C,155 (1984).
 - [13] P. Astone, G. V. Pallottino, G. Pizzella, “Resonant g.w. antennas for stochastic background measurement” *Classical Quantum Gravity*, 14, 2019-2030 (1997)
 - [14] P. Astone, M. Bassan, P. Bonifazi, P. Carelli, E. Coccia, C. Cosmelli, V. Fafone, S. Frasca, S. Marini, G. Mazzitelli, P. Modestino, I. Modena, A. Moleti, G.V. Pallottino, M. A. Papa, G. Pizzella, P. Rapagnani, F. Ricci, F. Ronga, R. Terenzi, M. Visco, L. Votano, “The gravitational wave detector NAUTILUS operating at T=0.1 K” *Astroparticle Physics* 7, 231 (1997).
 - [15] G. Prodi “Initial operation of the g.w. detector Auriga” *Proc. of the Second Edoardo Amaldi Conference on Gravitational wave Experiments*, ed. E. Coccia et al., World Scientific (1998) pp. 148-158.
 - [16] J. Livas “Broadband search techniques for Periodic sources of gravitational radiation” in “Gravitational Wave Data Analysis”, 217 ed. B. F. Schutz. Kluwer Academic Publishers (1989).
 - [17] C. La Posta, S. Frasca “Search for monochromatic g.w. with the GEOGRAV detector” *Il Nuovo Cimento* 14C, 235 (1991).
 - [18] see, for example, S. A. Tretter, “Introduction to discrete time signal processing”, John Wiley & sons, New York (1976)
 - [19] B. F. Schutz
“The detection of gravitational waves” (Max Plank Institut, AEI-003 1996)